Sādhanā (2019) 44:145
https://doi.org/10.1007/s12046-019-1119-8
© Indian Academy of Sciences

A non-linear ductile damage growth law at elevated temperature

MANOJ KUMAR[1,*], SACHIN S GAUTAM[2] and PRAKASH M DIXIT[3]

[1]Department of Mechanical Engineering, Dr. B R Ambedkar National Institute of Technology, Jalandhar 144011, India
[2]Department of Mechanical Engineering, Indian Institute of Technology, Guwahati 781039, India
[3]Department of Mechanical Engineering, Indian Institute of Technology, Kanpur 208016, India
e-mail: kumarm@nitj.ac.in; manojsinghkiran@gmail.com; ssg@iitg.ac.in; pmd@iitk.ac.in

MS received 29 January 2018; revised 24 February 2019; accepted 12 March 2019; published online 22 May 2019

Abstract. Continuum damage mechanics (CDM) model is commonly used for the prediction of ductile fracture. For numerical simulation of ductile fracture in impact or high-temperature problems, the damage growth law that incorporates the effect of high temperature is needed. Experimentally, it has been observed that damage growth decreases with temperature. However, the damage growth law at high temperature is not easily available in the literature. In the present work, a damage growth law at high temperature is proposed for steel, based on the experimental measurement of damage carried out at IIT Kanpur.

Keywords. Continuum damage mechanics; high-temperature ductile fracture; high-temperature damage growth; high-temperature tensile test; triaxiality; SEM.

1. Introduction

In continuum damage mechanics (CDM) model, the void density at a point is described by a continuum variable, called damage. This variable is introduced in the constitutive relation to include the material softening due to void growth. Then, the theory of continuum thermodynamics is used to derive the evolution law for damage growth (termed as the damage growth law) from the damage potential (a part of the dissipation potential). This damage growth along with the critical damage criterion is used to predict ductile fracture.

The damage growth law in references [1, 2], for *isothermal* case, has only one material constant S_0. The constant is expressed in four measurable quantities (i.e., the equivalent plastic strain and damage at the damage initiation and fracture) so as to express the damage as a linear function of strain in tension test [1]. However, this does not agree with the experimental variation for many steels, which is found to be non-linear. Since then, many non-linear damage growth laws, for isothermal case, have been proposed by various authors [3–8]. A non-linear damage growth law for isothermal case has been reported in reference [9] based on the experimental measurement of void growth [10] for three spheroidized steels [AISI 1015/1045/1090]. Recently, a non-linear damage growth law for isothermal case based on experimental measurement of void growth for IS 2062: 2006 GR E410W A steel has also been proposed [11].

It is well known that the mechanisms of void nucleation and growth are sensitive to temperature changes. At high temperature, the nucleation is affected by the change in the rate of the thermally activated nucleation mechanism while the growth gets affected due to the thermal softening of the material.

There have been quite a few attempts to develop an evolution equation for void growth by incorporating the thermal effects. Using heuristic considerations, in reference [12] a temperature-dependent model is postulated for the void nucleation in terms of the evolution equation for a porosity (void volume fraction) parameter. These models account for the interaction of voids. Further, in [12] a criterion is proposed that ductile fracture occurs whenever the hardening–softening parameter κ of the constitutive model of an elastic–viscoplastic voided solid becomes zero. A temperature-dependent yield stress is used to analyse a single spherical void in the matrix material subjected to external stress field in [13]. The evolution equation for void growth is obtained in terms of the rate of distention. The distension is defined as $b^3/(b^3 - a^3)$ where b is the matrix radius and a is the void radius. An expression for the threshold stress (i.e., the stress at the onset of void growth) is also obtained that depends on the distention, initial temperature, melting temperature, and initial yield stress. Numerical analysis shows that the threshold stress is less when the temperature dependence is incorporated. Further, the thermal effect on the void growth is more at high strain

*For correspondence

rates. The void growth models presented in [12] and [13] contain material functions of porosity or distention that are not very easy to determine. Hence, these evolution equations are not very convenient for numerical simulation of ductile fracture.

There have been attempts to include the thermal effects in the void growth or damage models that have been obtained earlier for room temperature. This effect has been incorporated in [14] by assuming the parameter n (which is the inverse of the strain rate sensitivity parameter) in the Cocks–Ashby void growth model to be temperature dependent. Experiments and finite-element (FE) simulations on AISI 304L stainless-steel notched specimen in tension test were conducted at high temperatures to obtain the variation of n with temperature. (For FE simulation, a plasticity model proposed by Horstemeyer and his coworkers that includes temperature-dependent isotropic as well as kinematic hardening is used.) It was observed that the parameter n decreases when the temperature increases from 800 to 1200 K. It was concluded that the Cocks–Ashby model needs an explicit dependence on the temperature. Also, it was observed that the void nucleation, growth and coalescence take place at different rates at higher temperature than at room temperature. The thermal effect was incorporated in some of the ductile fracture criteria that are based on the void nucleation and growth in [15]. In this model, the evolution equations for the void nucleation and growth depend on the nucleation and growth threshold stresses. The thermal effect is included by scaling the nucleation and growth threshold stress using the temperature-dependent shear modulus that is obtained from thermodynamic considerations. Also, the temperature dependence in the Tuler–Butcher-type dynamic fracture criteria was included, where the damage is considered as some function of the entire stress history and thus depends on the threshold stress. Again, the temperature dependence of the damage is incorporated by scaling the threshold stress using the temperature-dependent shear modulus, obtained from thermodynamic considerations.

In the framework of CDM model also, there are some attempts to include the thermal effect on the damage growth. The temperature-dependent yield stress was used [16] (given by the solid-state equation of Milella) to incorporate the thermal effect on some of the material parameters, appearing in the non-linear damage growth law proposed earlier [7]. The material parameters are the threshold strain (i.e., the equivalent plastic strain at the onset of damage), the fracture strain (i.e., the equivalent plastic strain at fracture) and the critical damage (i.e. the damage at fracture). Based on experiments on round notched bar in tension, a linear variation was proposed for these material parameters with the homologous temperature (i.e., a fraction of the melting point temperature on the Kelvin scale). However, the thermal effect on the remaining parameters is not investigated. Later, a temperature-dependent yield stress and the Lemaitre's damage growth law were used to find the variation of damage with temperature in steel by performing FE analysis and tension tests on notched specimens at high temperature [17]. However, the parameters in the Lemaitre's damage growth model are assumed to be temperature-*independent.* The critical total damage work was used as the fracture criterion. The FE analysis shows that damage decreases with temperature. However, no temperature-dependent damage growth law was proposed.

For quite some time, some empirical temperature-dependent ductile fracture criteria have been in use for the numerical simulation of ductile fracture. The most common of such criteria is due to Johnson and Cook (JC) [18]. Based on torsion tests on Hopkinson bars over a range of temperatures as well as some quasi-static tensile tests on notched specimens, the fracture strain was obtained as a function of the triaxiality, temperature and strain rate for OFHC copper, Armco iron and 4340 steel. The damage was defined as the cumulative equivalent plastic strain normalized by the fracture strain. Thus, fracture occurs whenever damage reaches unity. The proposed fracture model was evaluated by conducting cylinder impact tests and comparing the test results with the predicted values. It was reported that the fracture in the tests occurs earlier than the predicted values. A different function for the dependence of the fracture strain on temperature and strain rate for 30Cr2Ni4MoV ultra-super-critical steel was proposed in [19] by conducting tensile tests at different temperatures and strain rates. The model was evaluated by performing upsetting (cylindrical, tapered and double-cone) tests at higher temperature and comparing the fracture location and the reduction ratio (at which fracture initiates) to the predicted results from the simulation using DEFOERM-3D FE software by incorporating the proposed fracture model in it. It was reported that the agreement between the tests and the predicted results was good.

The literature survey shows that the empirical temperature-dependent ductile fracture criteria are not always accurate in predicting the fracture in impact problems or high-temperature problems. Thus, there is a need to develop temperature-dependent criteria that are based on the physics of the ductile fracture process: void nucleation, growth and final coalescence. There are a few attempts to develop temperature-dependent evolution equations for the void growth. However, the nature of the material functions involved in these evolution equations do not make them very convenient to use in numerical simulation of fracture. The number of studies to quantify the void (or damage) growth at high temperature that can be easily integrated in ductile fracture criteria (including those that use the framework of CDM) is small.

The present work focuses on the phenomenological modelling of ductile fracture using CDM theory, which has been established within the thermodynamic framework. The drawbacks of JC models have been widely reported; see for example the paper by Guo *et al* [20]. The limitations

of empirical models have been stated earlier. Hence, the motivation of the present work is to incorporate the temperature effects using the physics of the ductile fracture in the proposed criteria. Since almost all the works try to incorporate the effect of temperature empirically, the present work focuses to incorporate the effect of temperature through physics. Hence, it is expected that such an approach would be better than the empirical approach. The incorporation of the effects of the strain rate is left as a future work. A high-temperature ductile damage growth law for IS 2062: 2006 GR E410W A steel is proposed that can be used in the framework of CDM. The temperature-dependent material parameters are estimated from the void growth measurement in tension tests at the following temperatures: 300 (room temperature), 350, 425, 500 and 575 K. The technique of direct measurement of void growth [10] is employed for this purpose.

2. CDM and damage growth law

It is assumed that the damage (D) at a point is isotropic. Then, it is defined by the relation

$$D = \lim_{\Delta A \to 0} \left(\frac{\Delta A_v}{\Delta A} \right) \tag{1}$$

where ΔA is a small area surrounding the point in some plane and ΔA_v denotes the area of void traces within ΔA.

The dissipative part of the thermodynamic force $(-Y)$ corresponding to the damage rate is calculated as the strain energy release rate (due to damage) at constant stress [1, 2, 20]. It is given by

$$-Y = \frac{\sigma_{eq}^2}{2E(1-D)^2} f\left(\frac{\sigma_m}{\sigma_{eq}} \right) \tag{2}$$

where

$$f\left(\frac{\sigma_m}{\sigma_{eq}} \right) = \left[\frac{2}{3}(1+\nu) + 3(1-2\nu)\left(\frac{\sigma_m}{\sigma_{eq}} \right)^2 \right] \tag{3}$$

Here, E is Young's modulus, ν is Poisson's ratio, σ_m the mean part of the Cauchy stress tensor σ_{ij} and σ_{eq} is the equivalent stress related to the deviatoric part σ'_{ij} by the relation

$$\sigma_{eq} = \sqrt{\frac{3}{2}\sigma'_{ij}\sigma'_{ij}}. \tag{4}$$

The ratio $\left(\sigma_m / \sigma_{eq}\right)$ is termed as the triaxiality.

The equivalent plastic strain ε^p_{eq} is defined as

$$\varepsilon^p_{eq} = \int d\varepsilon^p_{eq}; \quad d\varepsilon^p_{eq} = \sqrt{\frac{2}{3} d\varepsilon^p_{ij} d\varepsilon^p_{ij}} \tag{5}$$

where $d\varepsilon^p_{eq}$ is the equivalent plastic strain increment and $d\varepsilon^p_{ij}$ is the plastic part of the incremental linear strain tensor.

The plastic potential for a damaged material at temperature T can be written as [1, 2, 20]

$$F = F_1\left(\sigma_{ij}, \varepsilon^p_{eq}, D, T\right) + F_D\left(-Y, \varepsilon^p_{eq}, D, T\right) \tag{6}$$

where F_1 is the plastic potential corresponding to yielding and hardening and F_D is the plastic potential associated with damage. When a material follows the von Mises yield criterion and hardens isotropically, then F_1 is given by

$$F_1(\sigma_{ij}, \varepsilon^p_{eq}, D, T) = \frac{\sigma_{eq}(\sigma_{ij})}{1-D} - \sigma_Y(\varepsilon^p_{eq}, T) \tag{7}$$

where $\sigma_Y(\varepsilon^p_{eq}, T)$ is the variable yield stress that is approximated by the following power law:

$$\sigma_Y(\varepsilon^p_{eq}, T) = \sigma_{Y0}(T) + K(T)(\varepsilon^p_{eq})^{n(T)} \tag{8}$$

Here, $\sigma_{Y0}(T)$ is the temperature-dependent initial yield stress and $K(T)$ and $n(T)$ are temperature-dependent hardening parameters. Note that F_1 becomes equal to the original form of the von Mises plastic potential when $D = 0$. In this case, F_D reduces to zero. From the plastic potential of Eq. (6), the flow rules (i.e., the elasto-plastic constitutive relation and the damage growth law in incremental form) are given by

$$d\varepsilon^p_{ij} = d\lambda \frac{\partial F_1}{\partial \sigma_{ij}} = \frac{d\lambda}{(1-D)} \frac{3\sigma'_{ij}}{2\sigma_{eq}} \tag{9}$$

$$dD = d\lambda \frac{\partial F_D}{\partial(-Y)}. \tag{10}$$

The inner product of the tensor equation (9) with itself and substitution of the definitions of σ_{eq} (Eq. (4)) and $d\varepsilon^p_{eq}$ (Eq. (5)) in the inner product lead to the following relation between $d\lambda$ and $d\varepsilon^p_{eq}$:

$$d\lambda = (1-D) d\varepsilon^p_{eq}. \tag{11}$$

With this expression of $d\lambda$, Eq. (10) for the damage growth law takes the form

$$dD = (1-D) \frac{\partial F_D}{\partial(-Y)} d\varepsilon^p_{eq}. \tag{12}$$

Based on the experimental measurement of void growth in tension test, for *isothermal* process, the following form for the damage potential (F_D) is suggested [11]:

$$F_D = \frac{a_0}{b_0(1-D)} \exp[b_0(-Y)]. \tag{13}$$

Thus, Eq. (12) gives the following damage growth law:

$$dD = a_0 \exp[b_0(-Y)] d\varepsilon^p_{eq}. \tag{14}$$

The material constants a_0 and b_0 were estimated from the experimental measurement of void growth. When b_0 is

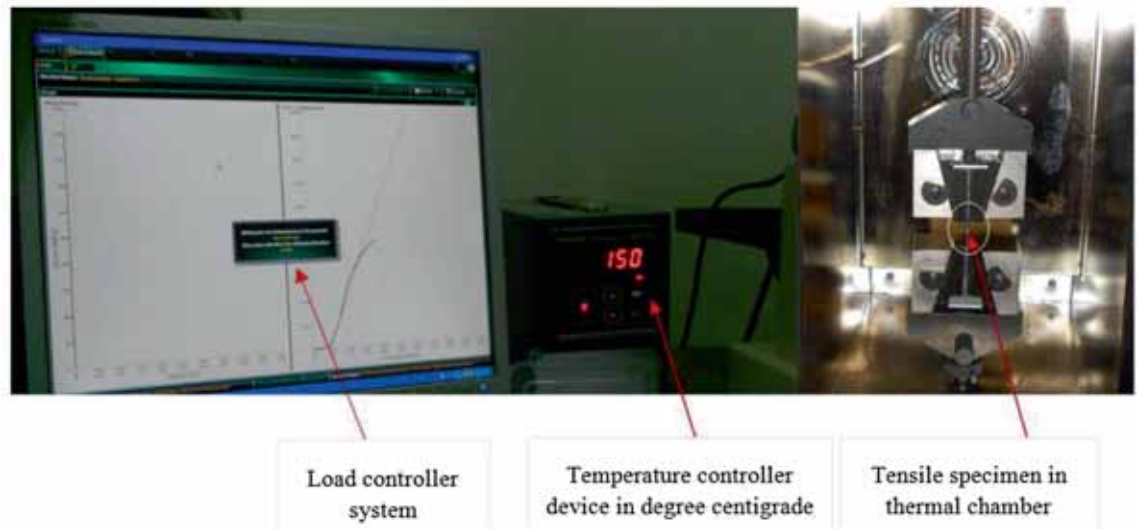

Figure 1. UTM (H10kT TINIUS OLSEN) with thermal chamber and temperature controller device.

zero, it gives a linear variation of damage with equivalent plastic strain.

3. Proposed damage growth law at high temperature

The isothermal damage potential of Eq. (13) can be modified for the case of high temperature in two different ways. In the first case, we treat the damage parameters a_0 and b_0 to be functions of temperature. Then, the damage potential becomes

$$F_D = \frac{a_0(T)}{b_0(T)(1-D)} \exp[b_0(T)(-Y)]. \tag{15}$$

Then, as per Eq. (12), the damage growth law takes the form

$$dD = a_0(T) \exp[b_0(T)(-Y)] d\bar{\varepsilon}^p_{eq}. \tag{16}$$

In this case, the temperature dependence of a_0 and b_0 is estimated from the experimental measurement of void growth in tension test at various temperatures. In the second case, a_0 and b_0 are kept constant at the room temperature level and the temperature dependence of damage is incorporated by a multiplicative function $f(T)$ in the expression (15) for the damage potential. Then, the damage potential and the corresponding damage growth law become

$$F_D = \frac{a_0}{b_0(1-D)} \exp[b_0(-Y)][f(T)] \tag{17}$$

$$dD = \left\{ a_0 \exp[b_0(-Y)] d\bar{\varepsilon}^p_{eq} \right\} [f(T)]. \tag{18}$$

In this case also, the material parameters of the function $f(T)$ are obtained from the experimental measurement of damage in tension test at various temperatures.

The experimental procedure for the measurement of void growth at various temperatures and the estimation of temperature dependence of the damage parameters $a_0(T)$ and $b_0(T)$ and the material function $f(T)$ are explained in the next section.

4. Experimental procedure for measurement of damage, triaxiality, equivalent plastic strain and equivalent stress at high temperature

The material used is IS 2062: 2006 GR E410W A steel, whose chemical composition is given in Appendix 1. The IS 2062: 2006 GR E410W A steel is a hot rolled and highly tensile structural steel. The steel possesess excellent weldability property, because of which it is employed in the boilers used in nuclear power plants. The cylindrical test specimens were kept in the thermal chamber of a 10-kN capacity UTM (H10kT TINIUS OLSEN) for 1 h and then tested in the displacement control mode to predefined plastic strain levels (5%, 10%, up to fracture). The UTM with thermal chamber and temperature controller device is shown in figure 1. Testing was done at 300 (room temperature), 350, 425, 500 and 575 K temperatures.

The procedure used in the present work to measure the damage, triaxiality, equivalent plastic strain and equivalent stress is very well established; see for example Berdin *et al* [21] and Lemaitre and Desmorat [22]. Also, the procedure has been shown to provide good correlation with the experimentally observed behaviour in static, see Dhar *et al* [23] and Gautam and Dixit [24], as well as strongly non-homogeneous deformation like impact problems, see Gautam and Dixit [25, 26]. Until now all the current works on ductile fracture using CDM use the data obtained at room temperature and uniaxial tension tests to simulate damage

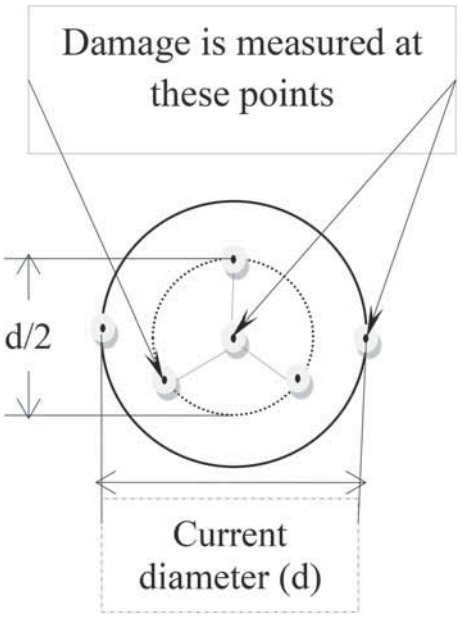

Figure 2. Locations of six representative surface elements.

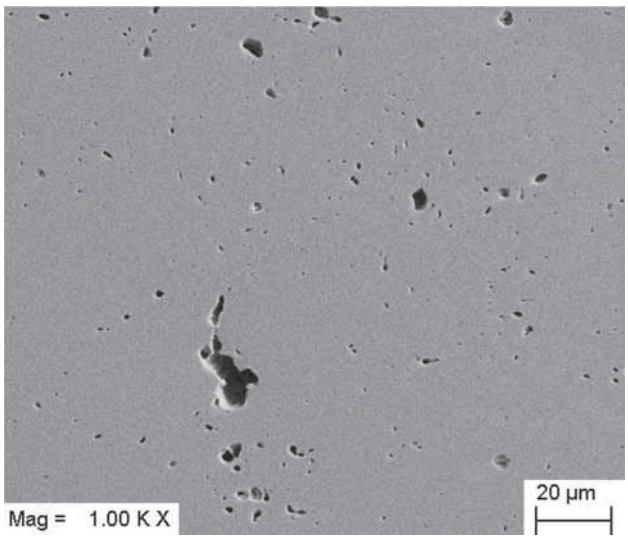

Figure 3. Magnified SEM images of a sample representative surface element.

growth in complex loading histories. The current work, for the first time, considers the effect of temperature on the damage growth law itself.

4.1 *Measurement of equivalent plastic strain*

The average equivalent plastic strain (at the minimum cross-section) is calculated as [11]

$$\varepsilon_{eq}^{p} = 2\ln\left(\frac{d_0}{d}\right) \tag{19}$$

where d_o and d are the initial and the current diameters of the cross-section, respectively. It is to be noted that the equivalent plastic strain cannot be found experimentally at the centre of the necking cross-section. Also, it has been found that the equivalent plastic strain is maximum at the centre of the necking zone and continuously decreases along the radial line. Hence, the average equivalent plastic strain is calculated using Eq. (19) at the necking cross-section.

4.2 *Measurement of damage*

As mentioned earlier, the direct method of void growth measurement [10] is employed in the present work. It is described in detail elsewhere [11]. Here, only some salient points have been reproduced. The damage is maximum at the centre of the necking zone and continuously decreases along the radial line. Hence, to calculate average damage variable D in this zone, six different locations are selected to find the average damage. The damage is measured at six representative surface elements (RSEs) on the polished surface (which coincides with the minimum cross-section of the necked zone) of thin samples. The locations of these surfaces are shown in figure 2. Based on the size of the defects, the characteristic dimension of RSE is chosen to be on the order of 200 × 200 µm. A high-resolution image (magnification factor of 1000) of each RSE is obtained at 20 kV using SEM imaging technique and an image processing program from the MATLAB. A magnified SEM image of a sample RSE is shown in figure 3. The damage D at an RSE is calculated as the ratio $\Delta A_v/\Delta A$ where ΔA is the RSE area and ΔA_v is the area of void traces within ΔA. Then, the average damage (D_{av}) at the polished surface is estimated as the average of the damage values over all the RSEs of the surface.

4.3 *Measurement of triaxiality*

The average triaxiality $(\sigma_m/\sigma_{eq})_{av}$ over the minimum cross-section is given by [27]

$$\left(\frac{\sigma_m}{\sigma_{eq}}\right)_{av} = \left\{\left[\left(1+\frac{2R}{a}\right)\ln\left(1+\frac{a}{2R}\right)\right]-\frac{2}{3}\right\} \tag{20}$$

where a is the radius of the cross-section and R is the radius of curvature of the necked profile at the cross-section. The value for R was calculated by first obtaining an image of necked profile using a microscope, then fitting a fourth-degree polynomial through the profile using a software and finally using a standard expression for the radius of curvature [11]. Once the necking starts, the effect of the nonhomogeneous deformation can be accounted based on the correction factor proposed in the work of Bridgman [27]. In the present work, this correction factor is used to

Table 1. Experimental values of necking parameters $A(T)$ and $B(T)$ (Eqs. (23) and (24)) at different non-dimensional temperatures T^*.

Temperature (K)	T^*	$A(T)$	$B(T)$
300	0	3.476	4.4
350	0.039216	3.882	4.801
425	0.098039	4.115	5.116
500	0.156863	4.226	5.297
575	0.215686	4.502	5.639

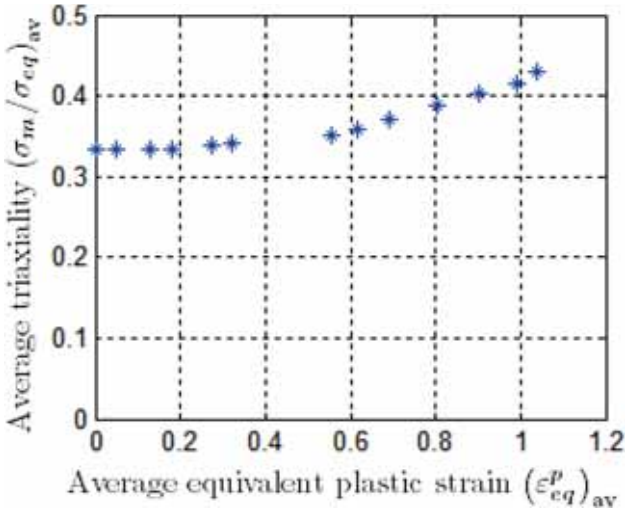

Figure 4. Experimental variation of average triaxiality with average equivalent plastic strain at room temperature (300 K).

take into account the effect of non-uniformity of the stress across the necking section.

Based on the experimental measurements, the ratio a/R after necking can be approximated as

$$\left(\frac{a}{R}\right) = \exp\left(A(T)\bar{\varepsilon}^p_{eq} - B(T)\right) \tag{21}$$

where the parameters $A(T)$ and $B(T)$ (called the necking parameters) depend on the temperature. Table 1 gives the values of the necking parameters at different non-dimensional temperatures T^* where T^* is defined as

$$T^* = \left(\frac{T - T_{RM}}{T_M - T_{RM}}\right) \tag{22}$$

Here, T_{RM} is room temperature (300 K) and T_M is the melting temperature of the material (1575 K). The values in table 1 suggest a linear dependence of the necking parameters A and B on the non-dimensional temperature T^*. Using the least-square method, this dependence can be expressed as

$$A(T) = 3.603 + 4.287(T^*), \tag{23}$$

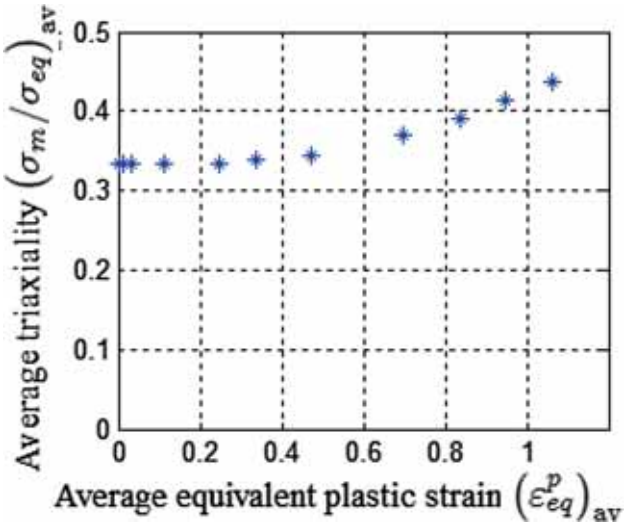

Figure 5. Experimental variation of average triaxiality with average equivalent plastic strain at 350 K.

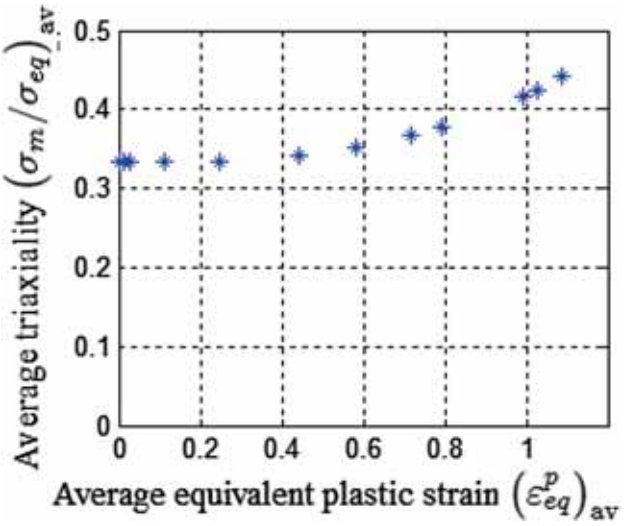

Figure 6. Experimental variation of average triaxiality with average equivalent plastic strain at 425 K.

$$B(T) = 4.504 + 5.353(T^*). \tag{24}$$

4.4 *Experimental results on average values of equivalent plastic strain, damage and triaxiality over the minimum cross-section in necked region*

Experimentally measured values of the average damage and average triaxiality at various levels of the average equivalent plastic strain are given in tables 8, 9, 10, 11 and 12 (Appendix 2) for temperatures of 300, 350, 425, 500 and 575 K, respectively.

The data from tables 8–12 (Appendix 2) are represented graphically in figures 4–8 and 9–13.

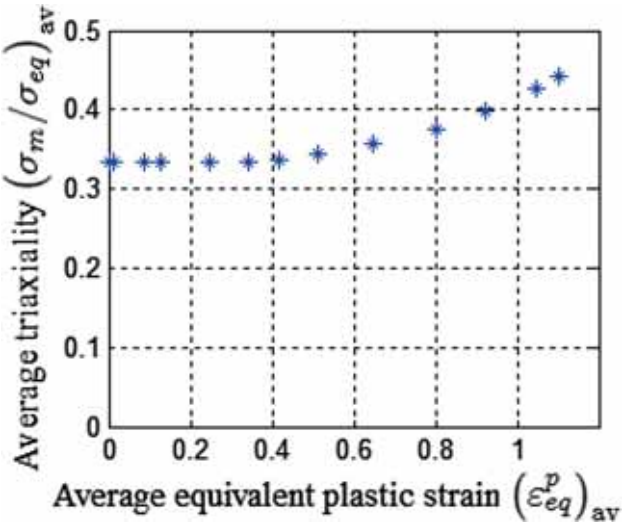

Figure 7. Experimental variation of average triaxiality with average equivalent plastic strain at 500 K.

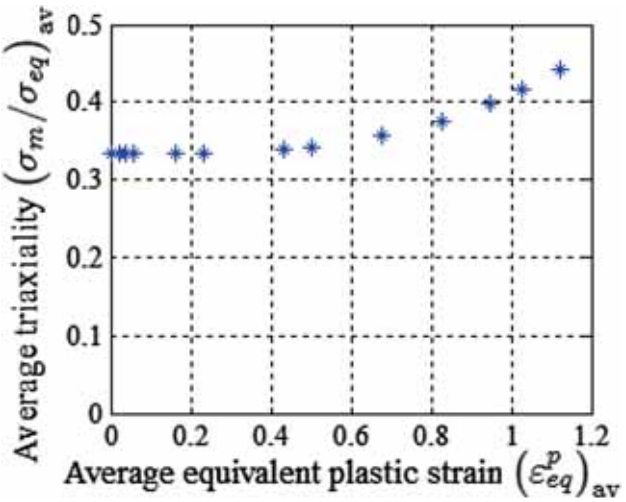

Figure 8. Experimental variation of average triaxiality with average equivalent plastic strain at 575 K.

Figures 4–8 show that, at a given level of (average) equivalent plastic strain, the (average) triaxiality decreases *slightly* with temperature after necking. The value of the (average) equivalent plastic strain up to which the (average) triaxiality remains constant is called the necking strain (ε_n). From these graphs, the dependence of the necking strain (ε_n) on the non-dimensional temperature T^* can be modelled by the following quadratic expression:

$$\varepsilon_n(T) = 0.240 + 0.035(T^*) + 0.401(T^*)^2 \qquad (25)$$

Figures 9–13 show that the growth of (average) damage with (average) equivalent plastic strain is slower at higher temperature.

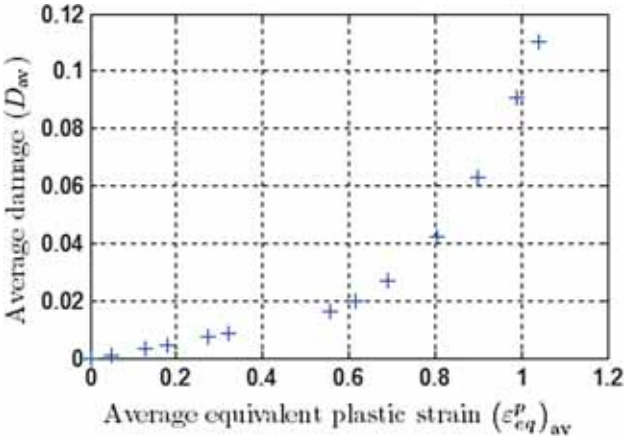

Figure 9. Experimental variation of average damage with average equivalent plastic strain at room temperature (300 K).

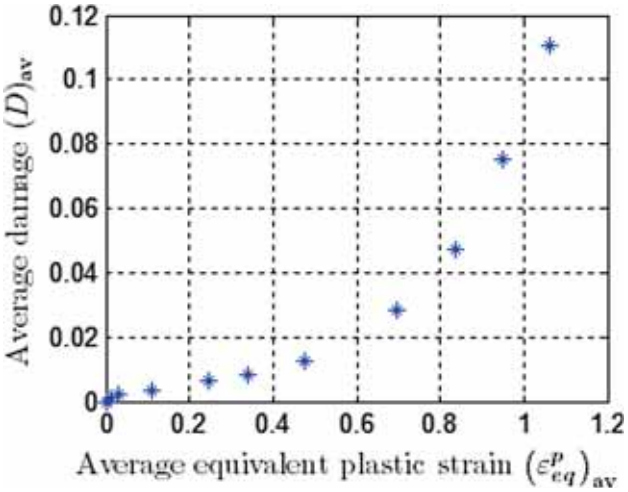

Figure 10. Experimental variation of average damage with average equivalent plastic strain at 350 K.

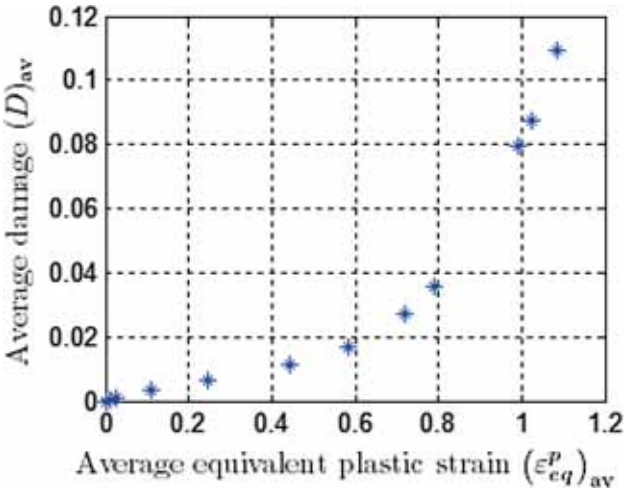

Figure 11. Experimental variation of average damage with average equivalent plastic strain at 425 K.

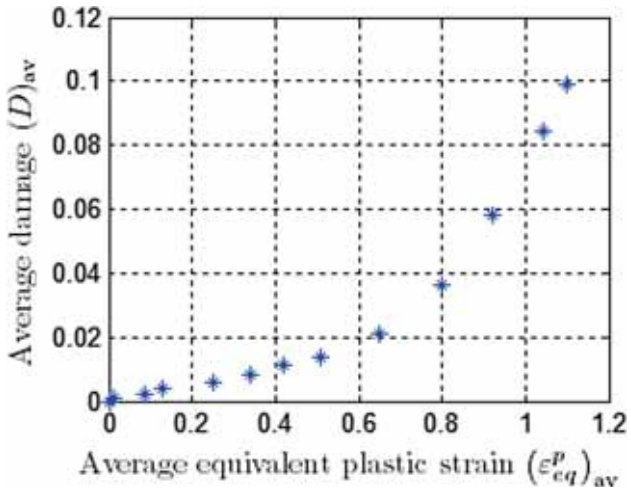

Figure 12. Experimental variation of average damage with average equivalent plastic strain at 500 K.

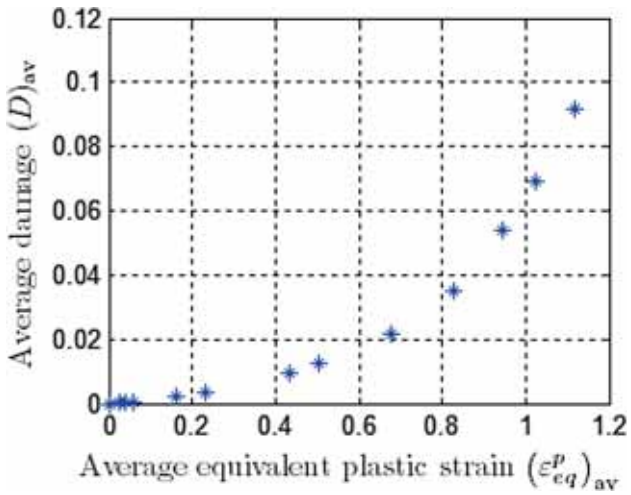

Figure 13. Experimental variation of average damage with average equivalent plastic strain at 575 K.

4.5 *Hardening relation*

First, the true stress is converted to the equivalent stress σ_{eq} at each level of the (average) equivalent plastic strain (ε_{eq}) [11] by multiplying the following correction factor [27]:

$$CF = \left(\frac{1}{\left(1+\frac{2R}{a}\right)\ln\left(1+\frac{a}{2R}\right)}\right). \tag{26}$$

Here, the ratio *a/R*, at each temperature, is obtained from Eqs. (21), (23) and (24). Then, the least-square method is used to fit the power law of Eq. (8) through the values of (σ_{eq},ε_{eq}) to obtain the hardening parameters $\sigma_{Y0}(T)$, $K(T)$ and $n(T)$ at different temperatures. These values are shown in table 2.

The values in table 2 suggest a quadratic dependence of the hardening parameters $\sigma_{Y0}(T)$, $K(T)$ and $n(T)$ on the non-dimensional temperature T^*. Using the least-square method, this dependence can be expressed as

Table 2. Experimental values of hardening parameters $\sigma_{Y0}(T)$, $K(T)$ and $n(T)$ of the power law (Eq. (8)) at different non-dimensional temperatures T^*.

Temperature (K)	Non-dimensional temperature T^*	Hardening parameters of power law (Eq. (8))		
		$\sigma_{Y0}(T)$	$n(T)$	$K(T)$
300	0	220	0.433	577
350	0.039216	218	0.449	558
425	0.098039	212	0.485	532
500	0.156863	205	0.52	495
575	0.215686	195	0.54	445

$$\sigma_{Y0}(T) = 220 - 48.36(T^*) - 314.2(T^*)^2, \tag{27}$$

$$K(T) = 577 - 316.6(T^*) - 1314(T^*)^2, \tag{28}$$

$$n(T) = 0.433 + 0.612(T^*) - 0.431(T^*)^2 \tag{29}$$

Finally, a graph of the equivalent stress versus the plastic part of the logarithmic strain at different temperatures is generated using the power law of Eq. (8) and these expressions for $\sigma_{Y0}(T)$, $K(T)$ and $n(T)$. The graph is shown in figure 14.

5. Determination of temperature dependence of $a_0(T)$ and $b_0(T)$ of Eq. (16) from experimental data

In order to determine the temperature dependence of the damage parameters $a_0(T)$ and $b_0(T)$, Eq. (16) is expressed as

$$\ln\left(\frac{dD}{d\varepsilon^p_{eq}}\right) = \ln(a_0(T)) + b_0(T)(-Y) \tag{30}$$

First, at each temperature, the difference formula

$$\ln\left(\frac{dD}{d\varepsilon^p_{eq}}\right)_{i+1} = \ln\left(\frac{D_{i+1}-D_i}{(\varepsilon^p_{eq})_{i+1}-(\varepsilon^p_{eq})_i}\right)(i=1,2,\ldots) \tag{31}$$

is used to calculate $\ln\left(dD/d\varepsilon^p_{eq}\right)$ at the level i+1 of (average) ε_{eq} using the data from tables 8–12. Then, the plastic potential F_1 (Eq. (7)) is set to zero and the hardening law (Eq. (8)) is used to express the equivalent stress (σ_{eq}) in terms of the hardening parameters $\sigma_{Y0}(T)$, $K(T)$ and $n(T)$:

$$\left(\sigma_{eq}\right) = (1-D)\left(\sigma_{Y0}(T) + K(T)(\varepsilon^p_{eq})^{n(T)}\right) \tag{32}$$

Next, Eq. (32) is used to eliminate σ_{eq} from expressions (2–3). As a result, the expression of the (average)

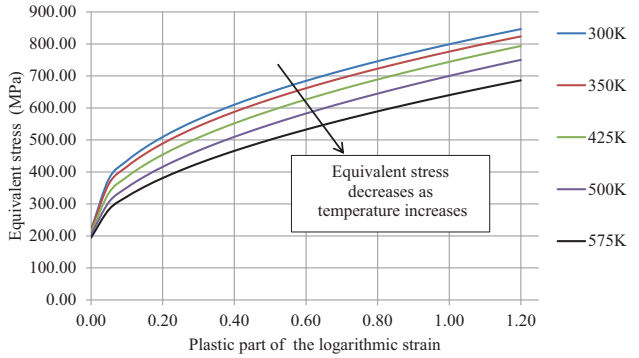

Figure 14. Graph of equivalent stress σ_{eq} versus the plastic part of logarithmic strain at different temperatures T.

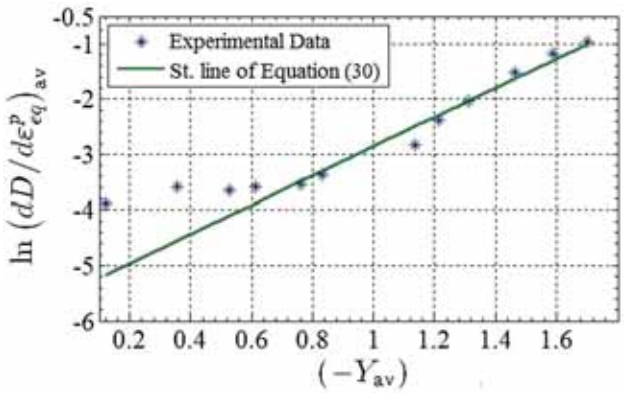

Figure 15. Graph of $\ln(dD/d\varepsilon^p_{eq})_{av}$ versus $(-Y)_{av}$ at room temperature (300 K) based on the average experimental values of table 13.

dissipative part of the thermodynamic force $(-Y)$ at the level $i+1$ of the equivalent plastic strain becomes:

$$(-Y)_{i+1} = \frac{1}{2E}\left[\sigma_{Y0}(T) + K(T)(\varepsilon^p_{eq})^{n(T)}_{i+1}\right]^2 \left[\frac{2}{3}(1+\nu) + 3(1-2\nu)\left(\frac{\sigma_m}{\sigma_{eq}}\right)^2_{i+1}\right] (i = 1, 2, \ldots) \tag{33}$$

Next, $(-Y)$ at the level $i+1$ is calculated from the above expression by taking the corresponding (average) values of the equivalent plastic strain (ε^p_{eq}) and triaxiality (σ_m/σ_{eq}) from tables 8–11 and those of the hardening parameters $\sigma_{Y0}(T)$, $K(T)$ and $n(T)$ from table 2. In Eq. (33), the elastic parameter $\nu(T)$ is assumed to be temperature-independent with the following value:

$$\nu(T) = 0.3. \tag{34}$$

Further, the decrease in the elastic parameters E (in GPa) with temperature T is estimated from the following relation:

$$E(T^*) = 200\left(1 - 0.2924(T^*) - 0.3796(T^*)^2\right) \tag{35}$$

which is obtained from the experimental data about steel [28] using the least-square method.

Tables 13–17 (Appendix 3) show the average values of $\ln(dD/d\varepsilon^p_{eq})$ and $(-Y)$, at different temperatures, calculated from Eqs. (31) and (33) using the experimental values of $(\varepsilon^p_{eq})_{eq}, (D)_{eq}$ and $(\sigma_m/\sigma_{eq})_{eq}$ of tables 8–12, the experimental values of $\sigma_{Y0}(T)$, $K(T)$ and $n(T)$ from table 2 and the values of $E(T)$ and $\nu(T)$ from Eqs. (34) and (35). It is observed that, at each level of (average) equivalent plastic strain, the (average) dissipative part of the thermodynamic force $(-Y)$ decreases with temperature.

Finally, Eq. (30) is fitted through the data of tables 13–17 by the method of least squares to obtain figures 15–19. In these figures, the natural logarithm of the damage parameter $a_0(T)$ is the intercept on the $\ln(dD/d\varepsilon^p_{eq})_{av}$ axis while the damage parameter $b_0(T)$ is the slope. The values of $a_0(T)$ and $b_0(T)$, at different temperatures, obtained from these figures are given in table 3.

The values in table 3 suggest a quadratic dependence of $a_0(T)$ on the non-dimensional temperature T^*. Using the least-square method, this dependence can be expressed as

$$a_0(T) = 0.0045 + 0.046(T^*)^2 \tag{36}$$

Here

$$T^* = \left(\frac{T - T_{RM}}{T_M - T_{RM}}\right) \tag{37}$$

where T_{RM} is room temperature (taken as 300 K) and T_M is the melting point temperature (taken as 1575 K). The plot of the least-square-fitted Eq. (36) is shown in figure 20 as solid line.

A similar procedure for the values for the parameter $b_0(T)$ suggests a linear dependence of $b_0(T)$ on the non-dimensional temperature T^*. Using the least-square method, this dependence can be expressed as

$$b_0(T) = 2.62 + 2.219(T^*). \tag{38}$$

The plot of the least-square-fitted Eq. (38) is shown in figure 21 as solid line.

It is observed that both the damage parameters $a_0(T)$ and $b_0(T)$ increase with temperature T. Further, if the room temperature values of a_0 and b_0 are used in the damage growth law of Eq. (16), it will lead to an *over*-estimation of the damage growth at higher temperature at the same level of equivalent plastic strain.

The damage growth law of Eq. (16) is integrated numerically:

$$D_{i+1} = D_i + \left\{a_0(T)\exp(b_0(T)(-Y)_i)\right\}\left(\left(\varepsilon^p_{eq}\right)_{i+1} - \left(\varepsilon^p_{eq}\right)_i\right) \quad (i = 1, 2, \ldots) \tag{39}$$

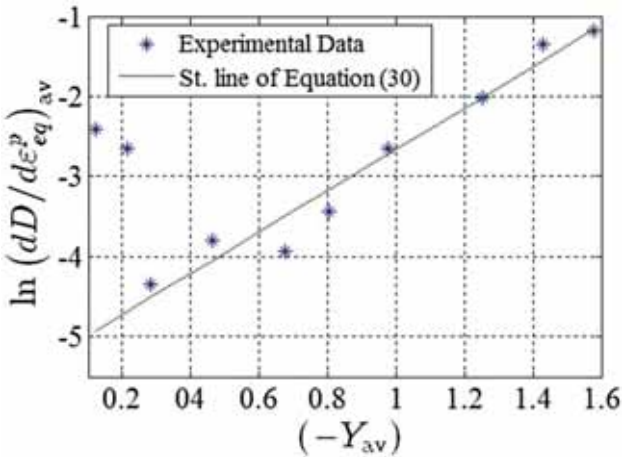

Figure 16. Graph of $\ln(dD/d\varepsilon^p_{eq})_{av}$ versus $(-Y)_{av}$ at 350 K based on the average experimental values of table 14.

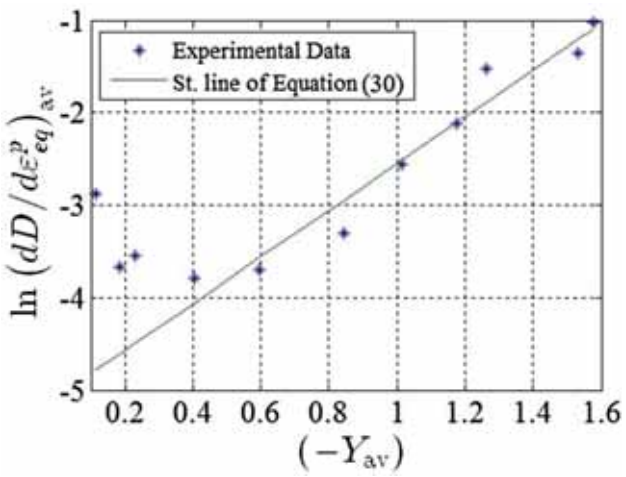

Figure 17. Graph of $\ln(dD/d\varepsilon^p_{eq})_{av}$ versus $(-Y)_{av}$ at 425 K based on the average experimental values of table 15.

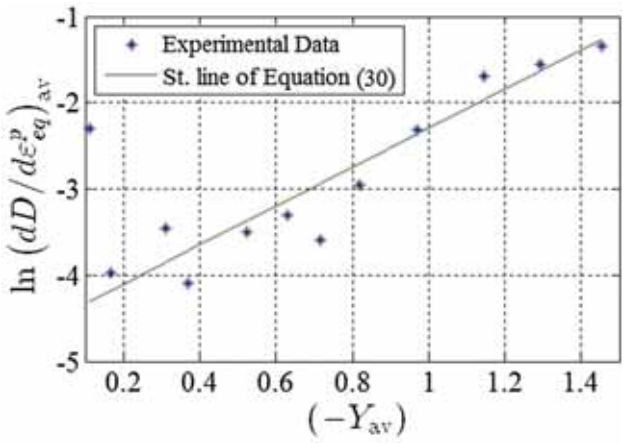

Figure 18. Graph of $\ln(dD/d\varepsilon^p_{eq})_{av}$ versus $(-Y)_{av}$ at 500 K based on the average experimental values of table 16.

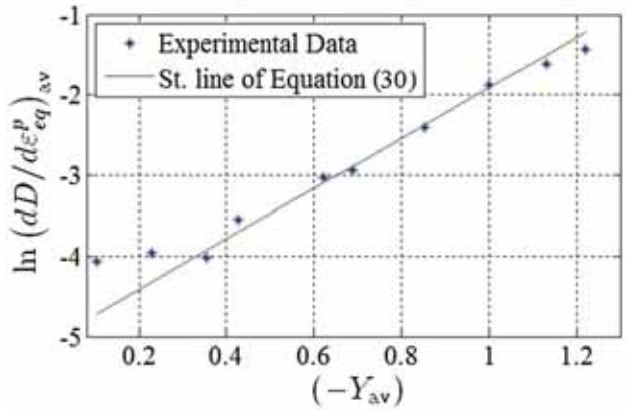

Figure 19. Graph of $\ln(dD/d\varepsilon^p_{eq})_{av}$ versus $(-Y)_{av}$ at 575 K based on the average experimental values of table 17.

to obtain the graph of the (average) damage versus the (average) equivalent plastic strain. Figures 22–26 show a comparison of these graphs with the experimental data of tables 8–12 for temperatures 300, 350, 425, 500 and 575 K. The agreement between the two is good. This implies that the proposed damage growth law (Eq. (16)) models the experimental trend of damage growth in IS 2062: 2006 GR E410W A steel at high temperatures well.

These graphs (figures 22–26), when extrapolated up to fracture, become almost vertical. Thus, approximate values of the critical damage (D_{cr}) at different temperatures can be obtained from these graphs as the values of damage at which the slope becomes equal to or greater than 10. The critical damage values for IS 2062: 2006 GR E410W A steel, as estimated from figures 21–25, are given in table 3. It is observed that the critical damage (D_{cr}) increases with temperature T. This implies, at higher temperature, that the ductile fracture would occur at higher level of damage.

The values in table 4 suggest a quadratic dependence of D_{cr} on the non-dimensional temperature T^*. Using the least-square method, this dependence can be expressed as

$$D_{cr}(T) = 0.42 + 0.32(T^*) + 2.626(T^*)^2. \qquad (40)$$

6. Determination of function $f(T)$ of Eq. (18) from experimental data

To determine the function $f(T)$ of Eq. (18) from the experimental data, this equation is first rearranged as

$$\frac{1}{\{a_0 \exp[b_0(-Y)]\}} \frac{dD}{d\varepsilon^p_{eq}} = f(T). \qquad (41)$$

Then, at temperatures 300, 350, 425, 500 and 575 K, the values of $\{1/a_0 \exp[b_0(-Y)]\}(dD/d\varepsilon^p_{eq})$ are calculated at different strain levels using the experimental data of $(-Y)$

Table 3. Calculated values of damage parameter at different temperatures from figures 15–19.

Temperature (K)	Non-dimensional temperature T^*	$a_0(T)$	$b_0(T)$ (MPa^{-1})
300	0	0.00450	2.62
350	0.039216	0.00466	2.72
425	0.098039	0.00487	2.85
500	0.156863	0.00550	2.94
575	0.215686	0.00650	3.12

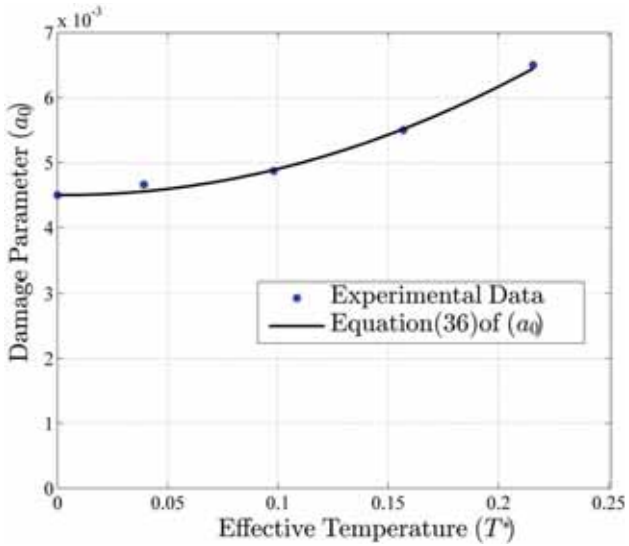

Figure 20. Variation of damage parameter (a_0) with T^* (effective temperature).

and $dD/d\varepsilon^p_{eq}$ from tables 13–17 and the values of a_0 and b_0 at room temperature from table 3:

$$a_0 = 0.0045,\ b_0 = 2.62\,(MPa)^{-1}. \tag{42}$$

Then, at each temperature, the mean value of the quantity $\{1/a_0 \exp[b_0(-Y)]\}(dD/d\varepsilon^p_{eq})$ over all the strain levels is obtained. As per Eq. (41), this mean can be considered as the experimental value of $f(T)$. Table 5 shows the experimental value of $f(T)$ at different non-dimensional temperatures.

Finally, the expression for $f(T)$ is obtained by fitting an appropriate function through the experimental values of table 5. These values suggest a power-law type of dependence on the non-dimensional temperature T^*:

$$f(T) = [1 + c_0(T^*)^m], \tag{43}$$

where the material constants c_0 and m, as determined from the least-square method, are

$$c_0 = 6.606, m = 1.178. \tag{44}$$

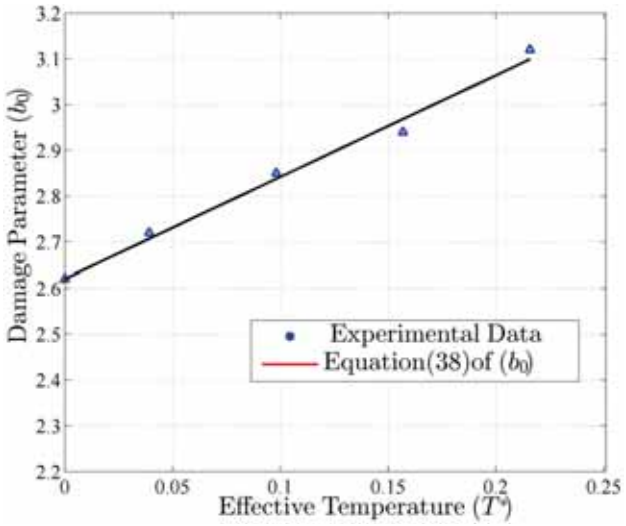

Figure 21. Variation of damage parameter (b_0) with T^* (effective temperature).

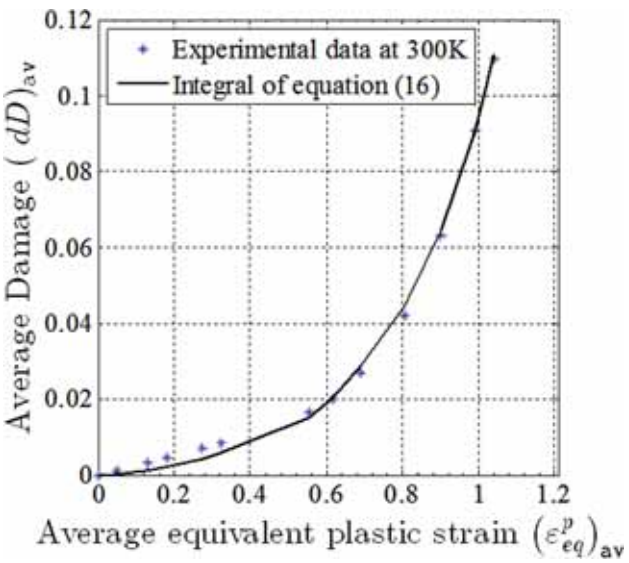

Figure 22. Comparison of the integral of the damage growth law of Eq. (16) with experimental data at room temperature (300 K) of table 8.

Thus, the proposed damage growth law at high temperature for IS 2062:2006 GR E410W A steel is

$$dD = \left\{a_0 \exp[b_0(-Y)]d\varepsilon^p_{eq}\right\}[1 + c_0(T^*)^m], \tag{45}$$

where the damage parameters a_0, b_0, c_0 and m are given by Eqs. (42) and (44).

The damage growth law of Eq. (45) is integrated numerically:

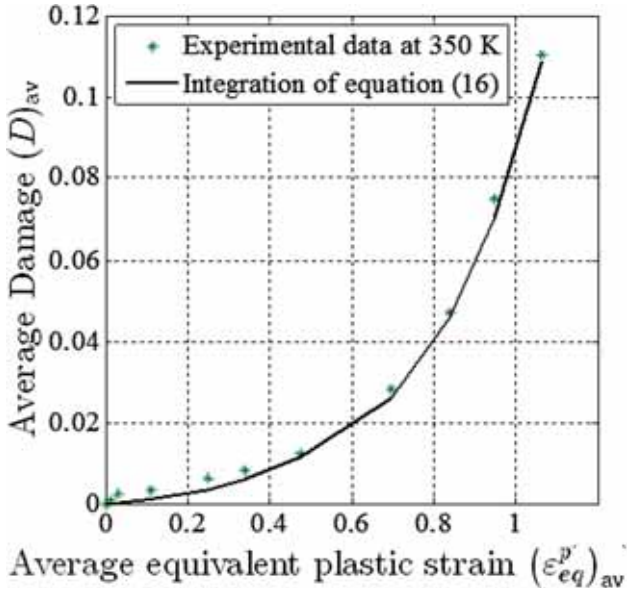

Figure 23. Comparison of the integral of the damage growth law of Eq. (16) with experimental data at 350 K of table 9.

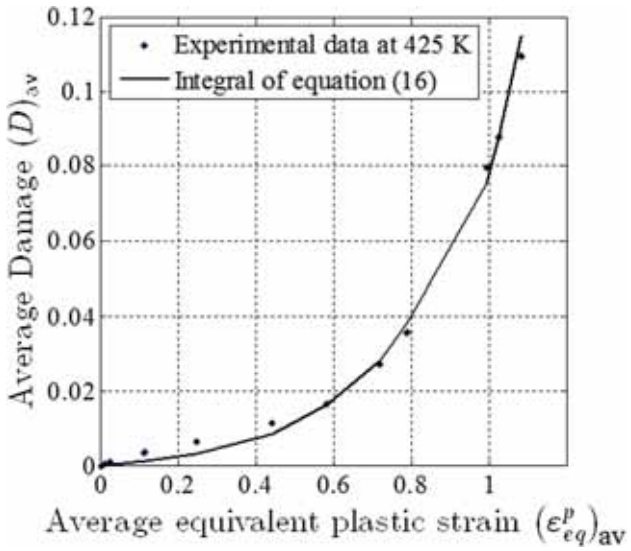

Figure 24. Comparison of the integral of the damage growth law of Eq. (16) with experimental data at 425 K of table 10.

$$D_{i+1} = D_i + \{a_0 \exp(b_0(-Y)_i)\}\left(\left(\varepsilon^p_{eq}\right)_{i+1} - \left(\varepsilon^p_{eq}\right)_i\right) [1 + c_0(T^*)^m](i = 1, 2, \ldots) \tag{46}$$

to obtain the graph of the (average) damage versus the (average) equivalent plastic strain. Figure 27 shows a comparison of the graph at temperature 575 K with the experimental data of table 12. In this case also, the agreement between the two is good. This implies that the second

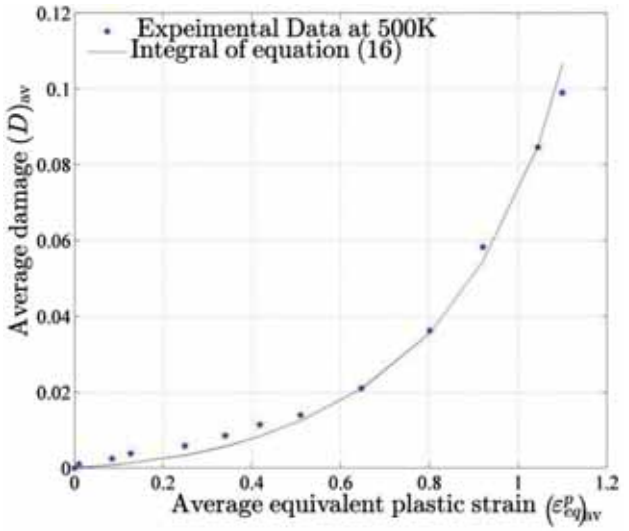

Figure 25. Comparison of the integral of the damage growth law of Eq. (16) with experimental data at 500 K of table 11.

Table 4. Values of critical damage at different temperatures estimated from figures 22–26.

Temperature (K)	300	350	425	500	575
Non-dimensional temperature T^*	0	0.039216	0.098039	0.156863	0.215685
Critical damage D_{cr}	0.42	0.43	0.48	0.53	0.61

version of the proposed damage growth law at high temperature (Eq. (44) where a_0, b_0, c_0 and m are given by Eqs. (41) and (43)) also models the experimental trend of damage growth in IS 2062: 2006 GR E410W A steel well.

The graph of the (average) damage versus the (average) equivalent plastic strain at $T = 575$ K corresponding to the first version of the proposed damage growth law of Eq. (16) (obtained from Eq. (39)) is reproduced in figure 27 for comparison. It is observed that the first version of the damage growth law of Eq. (16) (where $a_0(T)$ and $b_0(T)$ are considered to be functions of temperature T) has better agreement with the experimental results than the second version of damage growth law of Eq. (45) (where a_0 and b_0 are kept constant at the room temperature level and the temperature dependence is modelled by a multiplicative power law involving two additional material constants).

7. Demonstration of the predictive capability of the model

Next, the predictive capability of the model is demonstrated. This is done to show that the present model agrees with the experimental results over the range of temperature considered in the present work. Hence, to do this the data

Table 5. Experimental values of $f(T)$ calculated using Eq. (41), tables 13–17 and room temperature values of a_0 and b_0.

Temperature T (K)	Non-dimensional temperature T^*	Experimental value of $f(T)$
300	0	1.0000
350	0.039216	1.1500
425	0.098039	1.4037
500	0.156863	1.7229
575	0.215685	2.1444

Table 6. Calculated values of damage parameters using four different temperatures from tables (i.e., neglecting the data of 425 K).

Temperature (K)	Non-dimensional temperature T^*	$a_0(T)$	$b_0(T)$ (MPa^{-1})
300	0	0.00450	2.62
350	0.039216	0.00466	2.72
500	0.156863	0.00550	2.94
575	0.215686	0.00650	3.12

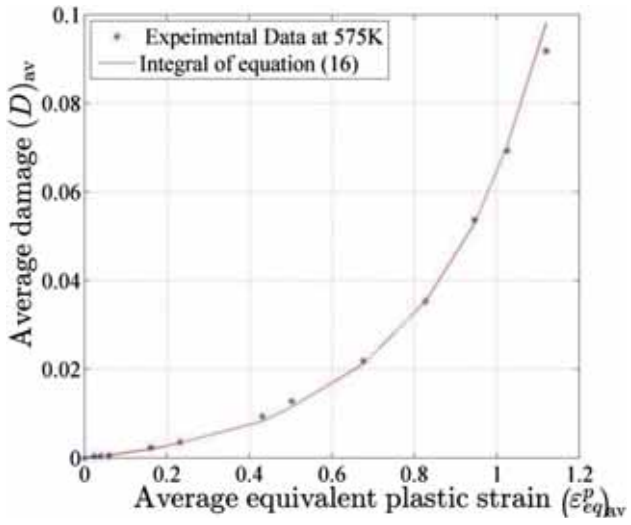

Figure 26. Comparison of the integral of the damage growth law of Eq. (16) with experimental data at 575 K of table 12.

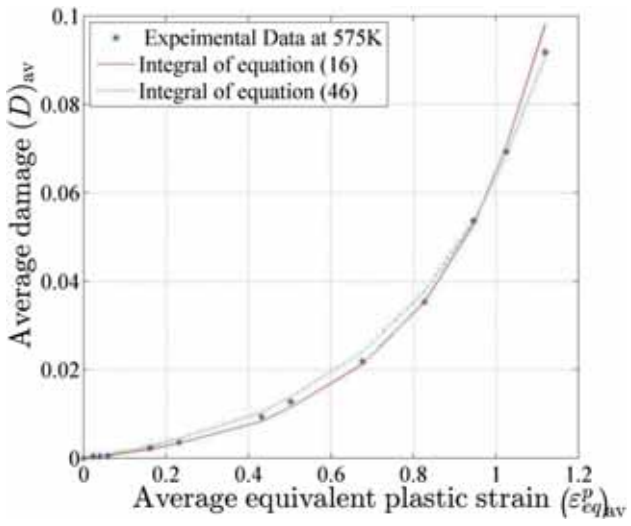

Figure 27. Comparison of the integrals of the damage growth laws of Eqs. (16) and (46) with experimental data of table 12 at 575 K.

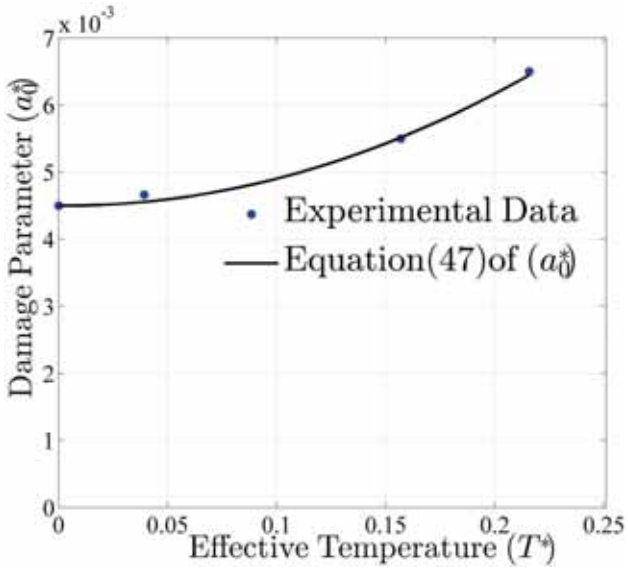

Figure 28. Variation of damage parameter (a_0^*) with T^* (effective temperature).

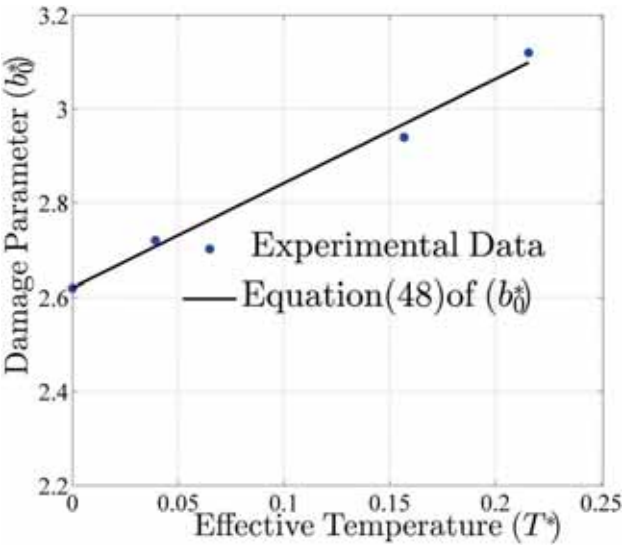

Figure 29. Variation of damage parameter (b_0^*) with T^* (effective temperature).

for temperature 425 K are removed and the values of the parameters a_0 and b_0 are shown in table 6 for four temperatures, viz. 300, 350 500 and 575 K; the least-square-fitted data for these parameters are shown in Eqs. (47) and (48), respectively. Figures 28 and 29 show the plot of Eqs. (47) and (48) alongside the values of table 6.

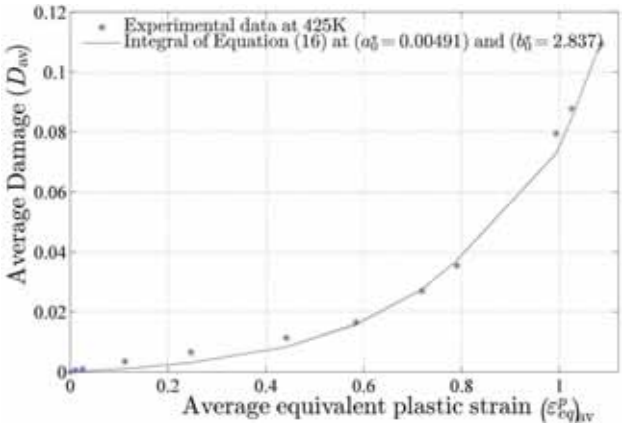

Figure 30. Comparison of the integrals of the damage growth laws of Eq. (16) at different damage parameters (a_0^*, b_0^*) at 425 K.

$$a_0^* = 0.0045 + 0.0432(T^*)^2 \tag{47}$$

$$b_0^* = 2.62 + 2.221(T^*) \tag{48}$$

The value of a_0^* and b_0^* at T = 425 K can be found using Eqs. (47) and (48) as 0.00491 and 2.837, respectively. Next, using Eq. (16) the predicted damage growth curve can be plotted against average equivalent plastic strain. This is shown in figure 30 alongside the experimental data obtained at 425 K. It can be seen that the present model is able to very accurately predict the damage growth at T = 425 K. Hence, it is clear that the proposed model will be able to capture damage growth, within the range of temperatures employed in the current work.

8. Conclusions

Two versions of a simple non-linear ductile damage growth law (for IS 2062: 2006 GR E410W A steel) are proposed at high temperature. In the first version, there are two temperature-dependent damage parameters $a_0(T)$ and $b_0(T)$. In the second version, these two damage parameters a_0 and b_0 are kept constant at the room temperature level and the temperature dependence of the damage is incorporated by a multiplicative power-law-type function of temperature. This function involves two additional material constants: c_0 and m. The temperature dependence of the two damage parameters in the first version and the four material constants appearing in the second version are estimated from the measurement of void growth in tension test (with thermal chamber) at the following temperatures: 300 (room temperature), 350, 425, 500 and 575 K. Further, a procedure to obtain an approximate value of the critical damage (at different temperatures), from the damage versus equivalent plastic strain graph, is suggested. The following observations can be made about this damage growth law:

- At a given level of equivalent plastic strain, the damage decreases when the temperature effect is included. This is because the dissipative part of the thermodynamic force ($-Y$) decreases with temperature at each equivalent plastic strain level.
- In the first version, both the damage parameters $a_0(T)$ and $b_0(T)$ increase with temperature. However, if the room temperature values of a_0 and b_0 are used in the first version of the damage growth law of Eq. (18), it leads to an *over*-estimation of the damage growth at higher temperature at the same level of equivalent plastic strain.
- The critical damage (D_{cr}) increases with temperature. This implies that, at higher temperature, the ductile fracture would occur at higher level of damage.
- The first version of the damage growth law has better agreement with the experimental results on damage growth.

Acknowledgement

The authors gratefully acknowledge Dr. C S Upadhyay, Dr. Rajesh Kitey and Dr. P M Mohite of the Structures Laboratory of the Department of Aerospace Engineering and Dr. Anish Upadhyay of the Physical Metallurgy Laboratory of the Department of Materials Science and Engineering, for providing the experimental facilities in the department. They would like to express their gratitude towards Dr. Sumit Basu and Dr. P Venkitanarayanan of the Department of Mechanical Engineering for their valuable guidance in the work at IIT Kanpur.

Appendix 1

The material used is IS 2062: 2006 GR E410W A steel, whose chemical composition (as determined by Spectro-Chemical Test: E415 – 2008, Standard Test Method for Atomic Emission Vacuum Spectrometric Analysis of Carbon Steel) is given in table 7.

Table 7. Chemical composition of IS 2062: 2006 GR E410W A steel.

% C	0.19	% Ni	0.01
% S	0.004	% Mo	0.01
% P	0.012	% Cu	0.01
% Mn	0.22	% V	0.01
% Si	0.07	% Carbon eq.	0.226
% Cr	0.018	% Al	0.024
Remaining % is Fe			

Appendix 2

Experimental values of average equivalent plastic strain, damage and triaxiality at different temperatures (See Tables 8–12).

Table 8. Experimental values of average equivalent plastic strain, damage and triaxiality at 300 K.

Level of average equivalent plastic strain (i)	Average equivalent plastic strain $(\varepsilon^p_{eq})_{av}$	Average damage D_{av}	Average triaxiality $(\sigma_m/\sigma_{eq})_{av}$
1	0	0.000	0.333
2	0.049	0.001	0.333
3	0.129	0.0032	0.333
4	0.179	0.0045	0.333
5	0.273	0.0071	0.338
6	0.321	0.0085	0.341
7	0.555	0.0165	0.352
8	0.615	0.020	0.358
9	0.69	0.027	0.371
10	0.804	0.042	0.389
11	0.90	0.063	0.403
12	0.99	0.091	0.415
13	1.04	0.11	0.431

Table 9. Experimental values of average equivalent plastic strain, damage and triaxiality at 350 K.

Level of average equivalent plastic strain (i)	Average equivalent plastic strain $(\varepsilon^p_{eq})_{av}$	Average damage D_{av}	Average triaxiality $(\sigma_m/\sigma_{eq})_{av}$
1	0.000	0.0000	0.333
2	0.010	0.0009	0.333
3	0.030	0.0023	0.333
4	0.111	0.0034	0.333
5	0.248	0.0064	0.333
6	0.339	0.0082	0.338
7	0.474	0.0125	0.345
8	0.698	0.0282	0.369
9	0.839	0.0470	0.391
10	0.948	0.0750	0.413
11	1.064	0.1106	0.438

Table 10. Experimental values of average equivalent plastic strain, damage and triaxiality at 425 K.

Level of average equivalent plastic strain (i)	Average equivalent plastic strain $(\varepsilon^p_{eq})_{av}$	Average damage D_{av}	Average triaxiality $(\sigma_m/\sigma_{eq})_{av}$
1	0.000	0.0000	0.333
2	0.010	0.0006	0.333
3	0.025	0.0009	0.333
4	0.112	0.0035	0.333
5	0.247	0.0065	0.333
6	0.442	0.0113	0.341
7	0.584	0.0165	0.353
8	0.719	0.0269	0.368
9	0.790	0.0355	0.378
10	0.993	0.0795	0.417
11	1.025	0.0877	0.425
12	1.085	0.1093	0.441

Table 11. Experimental values of average equivalent plastic strain, damage and triaxiality at 500 K.

Level of average equivalent plastic strain (i)	Average equivalent plastic strain $(\varepsilon^p_{eq})_{av}$	Average damage D_{av}	Average triaxiality $(\sigma_m/\sigma_{eq})_{av}$
1	0.000	0.0000	0.333
2	0.010	0.0010	0.333
3	0.085	0.0024	0.333
4	0.127	0.0037	0.333
5	0.249	0.0058	0.333
6	0.340	0.0085	0.334
7	0.418	0.0114	0.337
8	0.510	0.0139	0.343
9	0.647	0.0210	0.356
10	0.801	0.0362	0.375
11	0.921	0.0582	0.399
12	1.045	0.0846	0.426
13	1.100	0.0990	0.442

Table 12. Experimental values of average equivalent plastic strain, damage and triaxiality at 575 K.

Level of average equivalent plastic strain (i)	Average equivalent plastic strain $(\varepsilon^p_{eq})_{av}$	Average damage D_{av}	Average triaxiality $(\sigma_m/\sigma_{eq})_{av}$
1	0.000	0.000	0.333
2	0.024	0.000	0.333
3	0.039	0.000	0.333
4	0.059	0.000	0.333
5	0.161	0.002	0.333
6	0.232	0.004	0.333
7	0.432	0.009	0.338
8	0.503	0.013	0.341
9	0.677	0.022	0.356
10	0.827	0.035	0.375
11	0.946	0.054	0.399
12	1.025	0.069	0.417
13	1.120	0.092	0.443

Appendix 3

Values of natural logarithm of the slope and $(-Y)$ from the experimental data at different evaluated temperatures (See Tables 13–17).

Table 13. Calculated (average) values of natural logarithm of the slope and $(-Y)$ from the experimental data at 300 K of table 8.

Level of average equivalent plastic strain (i)	Natural logarithm of average slope $(dD/d\varepsilon^p_{eq})_{\text{av}}$	Average dissipative part of the thermodynamic force $(-Y)_{av}$ (MPa)
2	−3.8918	0.121
3	−3.5936	0.3568
4	−3.6497	0.5278
5	−3.5878	0.6145
6	−3.5347	0.7607
7	−3.3759	0.8294
8	−2.8416	1.1394
9	−2.3716	1.2162
10	−2.0281	1.3124
11	−1.5198	1.4612
12	−1.1676	1.591
13	−0.9676	1.7183

Table 14. Calculated (average) values of natural logarithm of the slope and $(-Y)$ from the experimental data at 350 K of table 9.

Level of average equivalent plastic strain (i)	Natural logarithm of average slope $(dD/d\varepsilon^p_{eq})_{\text{av}}$	Average dissipative part of the thermodynamic force $(-Y)_{av}$ (MPa)
2	−2.4079	0.1224
3	−2.6593	0.2132
4	−4.3457	0.2842
5	−3.8016	0.4617
6	−3.9286	0.677
7	−3.4467	0.8025
8	−2.658	0.9745
9	−2.0149	1.2522
10	−1.3591	1.4311
11	−1.1812	1.5776

Table 15. Calculated (average) values of natural logarithm of the slope and $(-Y)$ from the experimental data at 425 K of table 10.

Level of average equivalent plastic strain (i)	Natural logarithm of average slope $(dD/d\varepsilon^p_{eq})_{\text{av}}$	Average dissipative part of the thermodynamic force $(-Y)_{av}$ (MPa)
2	−2.8824	0.1161
3	−3.6756	0.1858
4	−3.5456	0.2323
5	−3.7869	0.4025
6	−3.7065	0.5972
7	−3.3072	0.8421
8	−2.5593	1.013
9	−2.1163	1.1754
10	−1.5286	1.2628
11	−1.3633	1.5302
12	−1.0217	1.5763

Table 16. Calculated (average) values of natural logarithm of the slope and $(-Y)$ from the experimental data at 500 K of table 11.

Level of average equivalent plastic strain (i)	Natural logarithm of average slope $(dD/d\varepsilon^p_{eq})_{\text{av}}$	Average dissipative part of the thermodynamic force $(-Y)_{av}$ (MPa)
2	−2.3026	0.1112
3	−3.9668	0.1655
4	−3.4563	0.3101
5	−4.098	0.3706
6	−3.5069	0.5244
7	−3.3094	0.6291
8	−3.5975	0.7162
9	−2.9557	0.8178
10	−2.3157	0.9695
11	−1.6951	1.1436
12	−1.5492	1.2913
13	−1.3381	1.4525

Table 17. Calculated (average) values of natural logarithm of the slope and $(-Y)$ from the experimental data at 575 K of table 12.

Level of average equivalent plastic strain (i)	Natural logarithm of average slope $(dD/d\bar{e}^{p}_{eq})_{\text{av}}$	Average dissipative part of the thermodynamic force $(-Y)_{av}$ (MPa)
2	−4.0697	0.1034
3	−6.5248	0.1753
4	−5.1761	0.2007
5	−4.0625	0.2302
6	−4.0197	0.3531
7	−3.5535	0.4276
8	−3.033	0.622
9	−2.9463	0.6886
10	−2.411	0.854
11	−1.8689	1.0018
12	−1.6203	1.1301
13	−1.4404	1.2204

References

[1] Lemaitre J 1985 A continuous damage mechanics model for ductile fracture. *ASME J. Eng. Mater. Technol*. 107: 83–89

[2] Lemaitre J 1996 *A course on damage mechanics*. Berlin: Springer-Verlag

[3] Tai W H and Yang B X 1986 A new microvoid damage model for ductile fracture. *Eng. Fract. Mech*. 25: 377–384

[4] Wang T J 1992 Unified CDM model and local criterion for ductile fracture I: unified CDM model for ductile fracture. *Eng. Fract. Mech*. 42:177–183

[5] Chandrakanth S and Pandey P C 1993 A new ductile damage evolution model. *Int. J. Fract.* 60: 73–76

[6] Chandrakanth S and Pandey P C 1995 An isotropic damage model for ductile material. *Eng. Fract. Mech*. 50: 457–465

[7] Bonora N 1997 A nonlinear CDM model for ductile failure. *Eng. Fract. Mech.* 58: 11–28

[8] Thakkar B K and Pandey P C 2007 A high-order isotropic continuum damage evolution model. *Int. J. Damage Mech.* 16: 403–426

[9] Dhar S, Sethuraman R and Dixit P M 1996 A continuum damage mechanics model for void growth and micro crack initiation. *Eng. Fract. Mech*. 53: 917–928

[10] LeRoy G, Embury J D, Edward G and Ashby M F 1981 A model of ductile fracture based on the nucleation and growth of voids. *Acta Metall*. 29: 1509–1522

[11] Kumar M and Dixit P M 2015 A nonlinear ductile damage growth law. *Int. J. Damage Mech*. 24: 1070–1085

[12] Perzyna P 1986 Internal state variable description of dynamic fracture of ductile solids. *Int. J. Solids Struct*. 22: 797–818

[13] Wang Z P 1994 Growth of voids in porous ductile materials at high strain rate. *J. Appl. Phys*. 76: 1535–1542

[14] Lu W Y, Horstemeyer M F, Korellis J S, Grishabar R B and Mosher D 1998 High temperature sensitivity of notched AISI 304L stainless steel tests. *Theor. Appl. Fract. Mech*. 30: 139–152

[15] Hanim S and Ahzi S 2001 A unified approach for pressure and temperature effects in dynamic failure criteria. *Int J Plasticity* 17: 1215–1244

[16] Bonora N and Milella P P 2001 Constitutive modeling for ductile metals behavior incorporating strain rate, temperature and damage mechanics. *Int. J. Impact Eng*. 26: 53–64

[17] Vaz Jr M, Munoz-Rojas P A and Lange M R 2011 Damage evolution and thermal coupled effects in inelastic solids. *Int. J. Mech. Sci*. 53: 387–398

[18] Johnson G R and Cook W H 1985 Fracture characteristics of three metals subjected to various strains, strain rates, temperatures and pressures. *Eng. Fract. Mech*. 21: 31–48

[19] He J, Cui Z, Chen F, Xiao Y and Ruan L 2013 The new ductile fracture criterion for 30Cr2Ni4MoV ultra-super-critical rotor steel at elevated temperatures. *Mater. Des*. 52: 547–555

[20] Guo Y B, Wena Q and Horstemeyer M F 2005 An internal state variable plasticity-based approach to determine dynamic loading history effects on material property in manufacturing processes. *Int. J. Mech. Sci*. 47: 1423–144

[21] Berdin C, Besson J, Bugat S, Desmoart R, Feyel F, Forest S, Lorentz E, Maire E, Pardoen T, Pineau A and Tanguy B 2004 *Local approach to fracture*. Paris: Les Presses de Le Ecole des Mines

[22] Lemaitre J and Desmorat R 2005 *Engineering damage mechanics: ductile, creep, fatigue and brittle failures*. Heildelberg: Springer-Verlag

[23] Dhar S, Sethuraman R and Dixit P M 1996 A continuum damage mechanics model for void growth and micro crack initiation. *Eng. Fract. Mech.* 53: 917–928

[24] Gautam S S and Dixit P M 2010 Ductile failure simulation in spherodized steel using a continuum damage mechanics coupled finite element formulation. *Int. J. Comput. Methods* 7: 319–348

[25] Gautam S S and Dixit P M 2011 Ductile fracture simulation in Taylor rod impact test using continuum damage mechanics. *Int. J. Damage Mech.* 20: 347–369

[26] Gautam S S and Dixit P M 2012 Numerical simulation of ductile fracture in cylindrical tube impacted against a rigid surface. *Int. J. Damage Mech.* 21: 341–371

[27] Bridgman P W 1952 *Studies in large plastic flow and fracture*. New York: McGraw Hill

[28] Kimball J A and Lovell D E 1925 Variation of Young's modulus with temperature from vibration measurements. *Phys. Rev.* 26: 121–124